Korean J. Chem. Eng., 39(3), 724-735 (2022)
DOI: 10.1007/s11814-021-0948-4

pISSN: 0256-1115
eISSN: 1975-7220

Influence of pore structure of granular activated carbon prepared from anthracite on the adsorption of CO_2, CH_4 and N_2

Bo Zhang*,†, Zhuoran Huang*, Ping Liu*, Jin Liu*, and Min Gu,†**

*College of Safety Engineering, Chongqing University of Science and Technology, Chongqing, 401331, P. R. China
**State Key Laboratory of Coal Mine Disaster Dynamics and Control, School of Resources and Safety Engineering, Chongqing University, Chongqing, 400044, P. R. China
(*Received 13 July 2021 • Revised 19 August 2021 • Accepted 1 September 2021*)

Abstract−A series of granular activated carbon (GAC) samples with similar surface chemical properties but different pore structures were prepared from anthracite. The maximum adsorption capacities of the prepared CO_2, CH_4, and N_2 at 298 K and 2.0 MPa were 4.27 mmol/g, 2.54 mmol/g, and 1.46 mmol/g, respectively, and the adsorption selectivity parameters, i.e., α_{CH_4,N_2} and α_{CO_2,CH_4}, were 3.23 and 3.06, respectively. By using the GAC with the optimum pore size as adsorbent, the concentration of methane in the nitrogen-methane (CH_4/N_2) mixture was concentrated from 30% to 63.5% via a single-column single-cycle pressure swing adsorption (PSA) process. The pore size distribution of the GAC samples was dominated by micropores, with specific surface area in the range of 330-500 m^2/g and micropore volume in the range of 0.12-0.19 cm^3/g. Although the specific surface area and pore volume of micropores played an important role in the separation performance, the pore size distribution was found to be the decisive factor. In particular, the micropores with sizes in the range of 5.0-10.0 Å were the main factor affecting the concentrating effect of CH_4 or CO_2 by GAC.

Keywords: Granular Activated Carbon, Pore Structure, CH_4 Enrichment, Adsorption Selectivity, Pressure Swing Adsorption

INTRODUCTION

Methane (CH_4), as the main component of coal mine gas, natural gas, and shale gas, is an important source of energy-producing relatively fewer CO_2 emissions compared to other fossil fuels. However, CH_4 is also a greenhouse gas, with a global warming potential over 20 times that of CO_2 [1]. Hence, the separation of CH_4/N_2 is very important in natural gas recovery. Generally, the methane content must be >90% to meet the requirements of pipeline delivery. In low-concentration coal mine gas, the CH_4 content is usually low, with many impurities, and is often mixed with large amounts of air. Therefore, the key to concentrating the CH_4 from low-concentration coal mine gas is in the separation of the CH_4/N_2 mixture [2]. Carbon dioxide (CO_2) is the main factor leading to the greenhouse effect, and is also an important raw material in chemical synthesis. CO_2 also has important applications in agricultural production, oil exploitation, and coal-bed methane extraction. Hence, the separation of CO_2/N_2 from flue gas has always been a focus of gas separation research. Among the different gas separation methods currently in use, pressure swing adsorption (PSA) is the most energy-saving and the lowest cost method. Previous studies have shown that PSA is a relatively ideal technical means for the separation of CH_4/N_2, CO_2/N_2, and CH_4/CO_2 mixtures [3]. Although this technology is relatively mature, the adsorbents used in gas separation have always been an important factor affecting its separation performance. One such adsorbent, activated carbon, is a carbon-based material composed of both microcrystalline and amorphous carbon, with characteristic large specific surface area and high adsorption capacity.

Research on the preparation of activated carbon and its application towards concentrating CH_4 and CO_2 has been ongoing for several decades. Twenty years ago, Lozano et al. [4] prepared activated carbon powder with a very high specific surface area of up to 3,290 m^2/g and a micropore volume of 1.45 cm^3/g from anthracite. Abdul et al. [5] prepared activated carbon using waste wood as the raw material, with a specific surface area of 1,139 m^2/g. Buczek et al. [6] conducted a systematic experimental study on the application of activated carbon towards concentrating CH_4 in coal seam gas. Their results showed that while larger adsorbent micropore volumes did not always result in better separation, the pore size played a very important role. Brea et al. [7] studied the penetration curves of mixed gases including CH_4, CO_2, N_2, and CO in composite beds using a variety of activated carbon samples. Their results revealed the competitive adsorption behavior of CH_4, CO_2 and N_2 mixtures in the PSA process. In recent years, the preparation of activated carbon via nitrogen doping has attracted significant attention worldwide. Researchers in Canada (Govind et al. [8]), South Korea (Park et al. [9] and Lee et al. [10]), and China (Wang et al. [11]) prepared nitrogen-doped activated carbon and studied the effects of its pore structure on CO_2 adsorption. However, these processes are not as environmentally friendly as physical activation. With the development of activated carbon preparation techniques, the preparation of activated carbon materials using raw materials as diverse as plant leaves [12] and even discarded drinks [13] has been reported. In comparison, although the new zeolite molecular sieves also show great potential towards the separation of CH_4,

†To whom correspondence should be addressed.
E-mail: zhangbo@cqust.edu.cn, mgu@cqu.edu.cn
Copyright by The Korean Institute of Chemical Engineers.

CO_2 and N_2 mixtures [14,15], the applications of activated carbon in fields as diverse as flue gas treatment, methane purification, adsorption and recovery of volatile organic compounds, prevention and control of air pollution, among others, have been widely studied [16-18]. However, while various studies have paid attention to the effects of the pore structure of activated carbon on CH_4 or CO_2 concentration, most of these do not feature an in-depth and systematic discussion on topics such as which pore size range plays a decisive role or on whether the surface chemistry of activated carbon also plays a role.

Against this backdrop, the present study prepared activated carbon materials that can efficiently concentrate CH_4 and CO_2, as well as to understand the pore structures and surface chemical properties of such materials at the micro level, in order to ensure its stable preparation at the macro level. To this end, granular activated carbon (GAC) was prepared from anthracite via an air pre-oxidation (or carbonization) physical activation process. First, the equilibrium separation effect of GAC on gas mixtures of CH_4/N_2, CO_2/N_2, and CH_4/CO_2 was studied by measuring the adsorption isotherms of these gases on GAC. Secondly, the concentrating effect of GAC on CH_4 in CH_4/N_2 mixtures was determined using a PSA technique. Finally, through characterization of the pore structure and surface chemical properties of GAC, the decisive factors affecting the separation performance of GAC were discussed.

MATERIALS AND METHODS

1. Raw Materials and Preparation of Activated Carbon

The raw coal used in this study was anthracite from the Chongqing and Ningxia regions of China. The method used for preparation of the GAC included the following six steps:

(1) Crushing the raw coal: first, the lumpy raw coal was broken up into particles with a size of <5 mm, which were then crushed into a ~160 mesh powder with the aid of a comminuter.

(2) Pre-oxidation: the coal powder was placed in a muffle furnace in contact with air and heated to 300-450 °C at a fixed heating rate, then held at the target temperature for 1 h, following which the preoxidized coal powder was removed from the furnace and cooled to room temperature.

(3) Powder molding: a certain mass of preoxidized coal powder was weighed in a fixed proportion with coal tar. After heating and melting the coal tar in an electric furnace, it was thoroughly mixed with the coal powder and a small amount of water, before being kneaded for 20-30 min. Finally, the mixture was poured into a molding machine to produce cylindrical particles of diameter of 3 mm and length 3-5 mm.

(4) Desiccation: the molded particles were placed into a drying oven and heated at a constant temperature of 105 °C for more than 4 h to fully remove any internal moisture present.

(5) Carbonization: the dried samples were placed in a muffle furnace and heated to 500-700 °C at a heating rate of 5-10 °C/min under an N_2 atmosphere, then held at the target temperature until fully carbonized.

(6) Activation: at 800-950 °C, a certain flux of activator (water vapor or carbon dioxide) was fully contacted with the carbonized material to activate the reaction. The activator flow was maintained for 1-4 h before being stopped. Once the temperature of the muffle oven dropped to room temperature, the samples were taken out, washed with water to remove any surface impurities present, then fully oven-dried to obtain the finished products.

2. Adsorption Isotherms

An IGA-100B intelligent gravimetric analyzer (Hiden Isochema, UK) was used to measure the GAC adsorption isotherms. Prior to the measurements, the adsorbent was pretreated, as follows: first, the mass of GAC sample to be tested was loaded into the balance chamber, which was then sealed and connected to an electric heating furnace. The samples were heated to 200 °C and held at this temperature for 10 h while a vacuum pressure was applied to the system. The purpose of the pretreatment is to fully remove any impurities present on the adsorbent surface, thereby allowing its true adsorption performance to be measured. After pretreatment, the system temperature was set to the adsorption temperature, and the pressure points to be measured were automatically predetermined by the IGA-100B instrument. Once the system temperature stabilized, the adsorption isotherms (up to maximum pressure of 2 MPa) and the kinetic curves at lower pressures were measured. Measuring the kinetic curves helps in gaining a quick understanding of the adsorption rules of N_2, CH_4, and CO_2 on the GAC samples in the shortest possible time, thereby providing a basis for the subsequent PSA concentration experiments.

3. Adsorption Selectivity

To compare the separation performance of different adsorbents, either laboratory-scale PSA cycle experiments can be carried out or mathematical models can be used for simulation. However, both these operations are time-consuming. Hence, a quick and simple calculation method for acquiring relevant parameters is needed to screen out the adsorbents that show better separation performance towards gas mixtures. The selection of appropriate adsorbent parameters should meet the following conditions: first, no complex calculations should be required, making the parameters relatively easy to estimate. Second, the parameters should reflect the isothermal adsorption characteristics under PSA operating conditions. Third, the parameters should reflect the selectivity of the adsorbents.

Here, a simple theory for the selection of parameters was used, based on the assumption that the adsorption isotherm satisfies Langmuir's equation. That is, the coverage rate of the adsorbent surface reaches its limit when the saturation adsorption pressure is reached, and the energy on the adsorbent surface is uniform. The Langmuir equation for a binary gas mixture is:

$$q_i=(q_{mi}b_ip_i)/(1+b_1p_1+b_2p_2) \quad (1)$$

where q_i and q_{mi} are the amount adsorbed and the maximum amount adsorbed of gas i, respectively; p is the pressure of the gas; and b_i is the adsorption coefficient.

The parameter for reflecting the selectivity for a binary system at adsorption equilibrium, $\alpha_{1,2}$, is defined as follows:

$$\alpha_{1,2}=(x_1/x_2)/(y_1/y_2) \quad (2)$$

where x_i and y_i are the mole fractions of component *i* in the adsorbed and gas phases, respectively. Generally, component 1 is considered as the one which is more easily adsorbed. Combining Eqs. (1) and

(2) shows that the adsorption selectivity towards component 1 is a constant over the entire range of adsorption pressures:

$$\alpha_{1,2}=(q_{m1}b_1)/(q_{m2}b_2) \quad (3)$$

The method shown here is only one of the many methods available for calculating the adsorption selectivity parameters (equilibrium separation coefficients) of adsorbents. For example, in their patent, Notaro et al. [21] proposed the definition of an empirical "preferred adsorption characteristic parameter" for the air separation process. Rege and Yang [22,23] proposed a simple parameter to compare the separation performance of binary gases by different adsorbents based on the equilibrium selectivity and adsorption capacity. In addition, Habgood et al. [24] expressed the selectivity parameter at short periods during dynamic separation as the square root of the ratio of the adsorption selectivity parameter to the diffusion coefficient; on this basis, Ruthven et al. [25] subsequently presented a method for calculating the dynamic selectivity parameters. These different approaches show that the methods used for calculating adsorption selectivity parameters depend on the characteristics of different absorbents. As the adsorption isotherms of the samples used in this study can all be described by the Langmuir equation, it is appropriate to use Eq. (3) to calculate the adsorption selectivity parameters in this case.

4. PSA Separation

The adsorption isotherms of CH_4 and CO_2 on GAC showed that while both these gases followed similar adsorption rules, the latter was more likely to be adsorbed. On the other hand, it is theoretically more difficult to separate CH_4/N_2 than CO_2/N_2 or CH_4/CO_2. Hence, in this study, priority was given to the PSA concentration of CH_4 in CH_4/N_2. The PSA experiments were conducted on a single-column and single-cycle pressure swing adsorption device designed and fabricated in-house [19].

The PSA process consisted of the following five steps:

(1) Pressurization: a CH_4/N_2 mixture containing ~29-31% CH_4 was injected into one end of the adsorption column, while the other end was kept closed to allow the pressure in the adsorption column to reach the target adsorption pressure.

(2) High pressure adsorption: the inlet and outlet air of the adsorption column were kept at an inflow and a venting state, respectively, and the pressure in the adsorption column was maintained at the pre-determined pressure before starting the adsorption process.

(3) Forward depressurization: the pressure of the adsorption column was reduced according to the direction of airflow in the adsorption process; consequently, the concentration of CH_4 near the outlet of the adsorption column gradually increased, while that of N_2 decreased.

(4) Backward depressurization: the pressure of the adsorption column was reduced to atmospheric, allowing the gas in the column (including the desorbed CH_4) to be released from the inlet end of the column and then collected as product gas.

(5) Backward vacuum-pumping: the pressure was further reduced to desorb as much of the CH_4 as possible, allowing the concentrated CH_4 product gas to be obtained and the adsorbent to be regenerated. Finally, the PSA concentration rate (ΔC_V) of CH_4 was calculated by subtracting the CH_4 concentrations in the feed and product gas.

$$\Delta C_V=C_p-C_f \quad (4)$$

where C_p is the average concentration of the effluent during backward vacuum-pumping step and C_f is the feed concentration of CH_4.

5. Pore Structure of Activated Carbon

The pore structure of the activated carbon was measured using an ASAP 2020M specific surface area and microporous analyzer (Micromeritics, USA). The samples were first dried and desorbed at 150 °C for 6 h, following which the adsorption isotherms were measured at the liquid nitrogen temperature (77 K) over a relative pressure range of 10^{-6}-1 using N_2 as the test gas. From the adsorption isotherm data, the specific surface area, S_{BET}, micropore surface area, S_{mic}, micropore size and volume, V_{mic}, distribution of micropore size, and total pore distribution in the range of 0.4-300 nm were obtained using the analysis software of the ASAP 2020M.

6. Surface Chemical Properties

FT-IR (Fourier transform infrared) spectra of GAC were obtained using a Nicolet MagnaIR550II FT-IR spectrometer (Thermo Fisher, USA) with pellets of GAC. The resolution was 4 cm^{-1} in the range from 1,000-4,000 cm^{-1}.

RESULTS AND DISCUSSION

1. Adsorption Isotherms of GAC

The selected activated carbon samples included CF-30 and TC-04, each activated by water vapor, and CF-91 and CF-80, each activated by carbon dioxide. The adsorption isotherms of CH_4, N_2, and CO_2 on each sample were measured at 298 K, at a maximum adsorption pressure of 2 MPa. The results are shown in Fig. 1, where it can be seen that the adsorption isotherms on all four samples are type I isotherms. The order of the adsorption capacities of CH_4, CO_2, and N_2 on CF-30, TC-04, and CF-91 were $CO_2>CH_4>N_2$, while that on CF-80 was $CO_2>N_2>CH_4$. In particular, the adsorption isotherm of CH_4 on CF-80 is linear at low pressures, but follows type I isotherm behavior as the pressure increases, before eventually reaching equilibrium. During this adsorption process, the adsorbed quantity of CH_4 is always less than that of N_2. These results show that in theory the adsorption properties of CF-80 are very helpful for the dynamic separation of CH_4/N_2 mixtures.

It is necessary to select appropriate theoretical models for analyzing adsorption isotherms. Although the Langmuir equation is relatively simple and does not have a strict theoretical thermodynamic basis (unlike the D-A equation, for instance), it often does a good job of descibing a variety of adsorption processes. As a result, this equation is widely applied both in theory and in engineering practice. To compare the activated carbon prepared here with commercially available types, the adsorption isotherms of Norit® RX3 and RB3 activated carbons were also used to calculate fitting parameters for the Langmuir equation. Fig. 1 shows the fitting results for the adsorption curves of CF-30, TC-04, CF-91, and CF-80, where it can be seen that the predicted values are consistent with the experimental data. The corresponding data for RX3 and RB3 are shown in Fig. 2. The calculated fitting parameters for CF-30, TC-04, CF-91, CF-80, RX3, and RB3 are shown in Table 1.

These results also show that the order of the adsorption capaci-

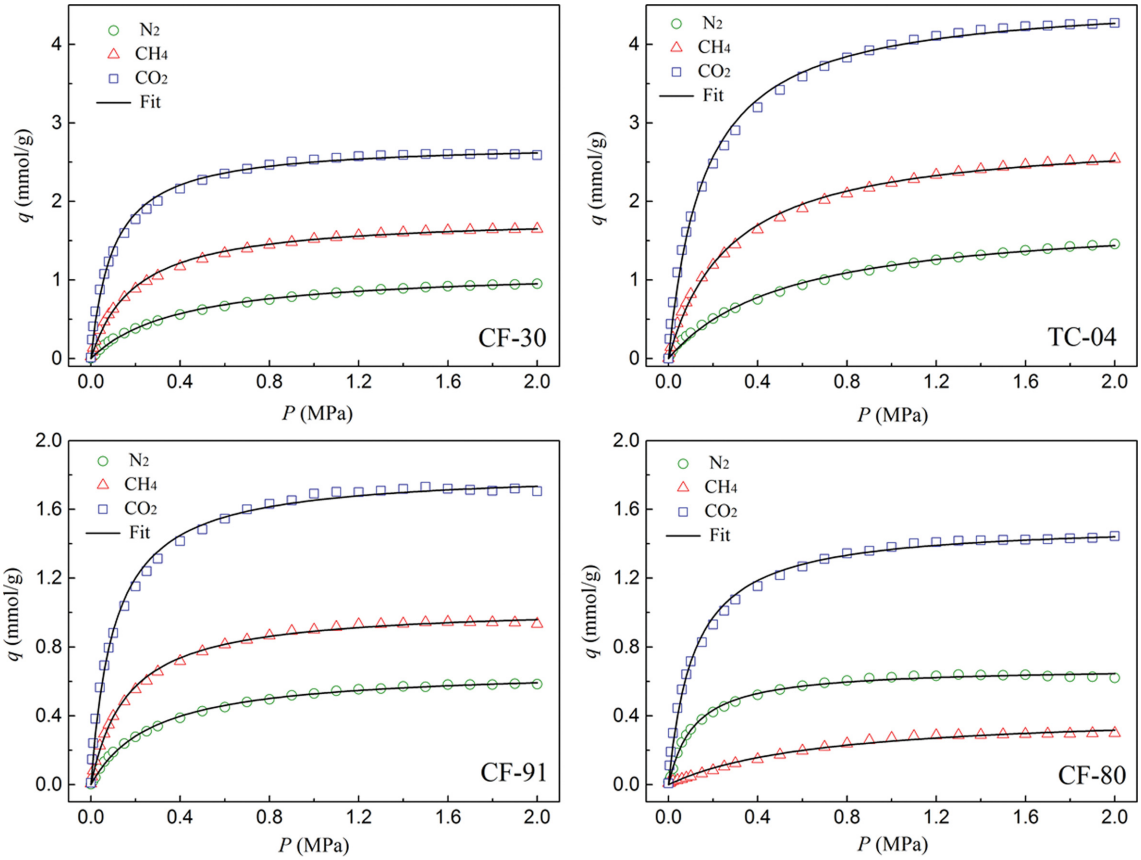

Fig. 1. Adsorption isotherms of CH_4, N_2, and CO_2 on CF-30, TC-04, CF-91, and CF-80 at 298 K.

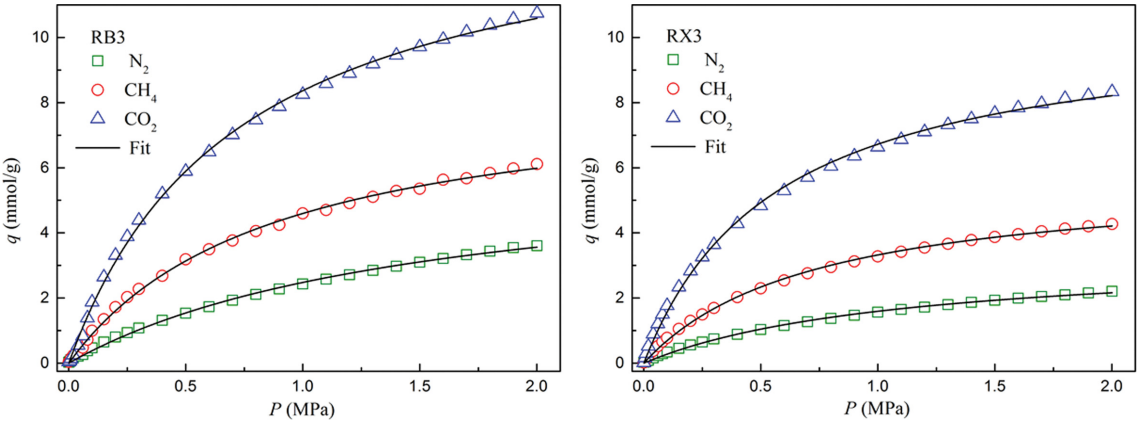

Fig. 2. Adsorption isotherms of CH_4, N_2, and CO_2 on Norit® RB3 and RX3 at 298 K.

ties of CH_4, CO_2, and N_2 on RX3 and RB3 were also CO_2>CH_4>N_2, and that the adsorption capacities of RX3 and RB3 were much larger than those of CF-30, TC-04, CF-91, and CF-80. Moreover, when the adsorption pressure reached 2 MPa, there was no obvious plateau stage, indicating the presence of a certain gap between the samples prepared in this study with the commercial activated carbon in terms of porosity and specific surface area. Although CF-30 and TC-04 showed better separation performance, their lower adsorption capacities resulted in a lower PSA gas handling capacity compared to the commercial activated carbon.

CF-80 is a special sample, and its adsorption behavior is similar to that of a carbon molecular sieve [20]. Its adsorption capacity for CH_4 is less than that for N_2, and increases very slowly with increasing pressure, with an obvious plateau appearing on the adsorption isotherm. Further, its adsorption capacity is the smallest of all the GAC samples, and only shows kinetic effects at the low pressure stage. At pressures >0.4 MPa, the adsorption for both CH_4 and N_2 both enters into the equilibrium state, indicating the presence of fewer pores capable of gas adsorption and a very small specific surface area in CF-80. Hence, the main similarity between the CF-

Table 1. Fitting results for the adsorption isotherms of CF-30, TC-04, CF-91, CF-80, RX3, and RB3 using the Langmuir equation

Sample	Gas	q_m (mmol/g)	b (MPa^{-1})	r
CF-30	N_2	1.14	2.51	0.999
	CH_4	1.81	5.11	0.998
	CO_2	2.75	10.29	0.997
TC-04	N_2	1.82	1.86	0.998
	CH_4	2.86	3.65	0.998
	CO_2	4.60	6.32	0.998
CF-91	N_2	0.67	3.59	0.999
	CH_4	1.04	6.12	0.999
	CO_2	1.82	9.65	0.998
CF-80	N_2	0.68	8.72	0.998
	CH_4	0.42	1.47	0.996
	CO_2	1.52	8.87	0.998
RX3	N_2	5.64	0.71	0.999
	CH_4	7.30	1.64	0.997
	CO_2	11.9	2.03	0.999
RB3	N_2	6.31	0.65	0.999
	CH_4	8.57	1.16	0.999
	CO_2	14.4	1.38	0.999

80 sample and the carbon molecular sieve is that they both have lower adsorption capacity for CH_4 than that for N_2, and show kinetic separation effects in the initial stage of adsorption. Nevertheless, the specific surface area and micropore content of the CF-80 sample are less than those of a commercial carbon molecular sieve.

As Table 1 shows, the orders of the q_m values for CF-30, TC-04, and CF-91 samples were all CO_2>CH_4>N_2, while that for CF-80 was CO_2>N_2>CH_4. These results are consistent with the adsorption curves, for which the value of the adsorption constant b follows the same trend. The value of b is related to the slope of the adsorption isotherm at the initial stage. The higher the value of b, the larger the slope. The b values of the CF-30, TC-04, and CF-91 isotherms for CH_4 were about twice those for N_2, while the b value of the CF-80 isotherm for N_2 was nearly six times that for CH_4. This indicates an obvious difference between the adsorption rates of CF-80 towards N_2 and CH_4 at the low pressure stage due to a kinetic-steric hindrance effect. Therefore, understanding the adsorption characteristics of adsorbents towards different gases is helpful in designing effective PSA experimental protocols and thereby reducing the number of experiments required. For the commercial activated carbon samples, the q_m values were significantly greater than those of the prepared samples, but the b values were relatively small, indicating that while the saturated adsorption capacity of these two commercial samples is large, the adsorption rates in the initial stages of adsorption may be smaller than those of CF-30 and TC-04.

2. Adsorption Selectivity Parameters

Previous studies have shown that α_{CH_4,N_2} of activated carbon is mostly <5.0. For example, α_{CH_4,N_2} of T103 activated carbon is 2.9 [26], which can be increased to 4.0 on modified activated carbon [27]. α_{CO_2,N_2} on activated carbon obtained by Ruan et al. [29] was in the range of 5-7. Foeth et al. [30] calculated α_{CO_2,CH_4} on activated carbon, with values reaching up to 3.5. However, some very high selectivity parameters have also been reported. For example, α_{CH_4,N_2} of AX-21 super activated carbon is 20.13, and that of shell activated carbon is 12.93 [28]. However, to date, these high-selectivity activated carbons have not been applied to the PSA process. Despite this, a greater value of $\alpha_{1,2}$ does not always imply better separation performance. Through an experimental study, and in conjunction with Ruthven et al. [32]'s work, Jasra et al. [31] concluded that when $\alpha_{1,2}$ was <2, the gas mixture was difficult to separate when the $\alpha_{1,2}$ was between 2 and 3; some separation could be achieved when the $\alpha_{1,2}$ was >3, the separation process was economical, and that when the $\alpha_{1,2}$ was >4, the increase of the $\alpha_{1,2}$ had no significance. These results indicate that the optimal $\alpha_{1,2}$ is between 3 and 4. The calculation results for $\alpha_{1,2}$ obtained using the data in Table 1 are shown in Table 2.

Table 2. Adsorption selectivity parameters of different samples

Sample	α_{CH_4,N_2}	α_{CO_2,N_2}	α_{CO_2,CH_4}
CF-30	3.23	9.89	3.06
TC-04	3.08	8.59	2.78
CF-91	2.65	7.30	2.76
CF-80	0.11	2.27	21.84
RX3	2.99	6.03	2.02
RB3	2.42	4.84	1.99

Table 2 shows that α_{CH_4,N_2} of CF-30 and TC-04 were in the desired range, indicating that these two samples can be used to separate the CH_4/N_2 mixture economically. On the other hand, the α_{CH_4,N_2} value of CF-91 was 2.65, meaning it can technically be used for the separation of the CH_4/N_2 mixture but the resulting process will not be economical, which is further confirmed by the PSA results and the adsorption curve data also confirm this. In the case of CF-30 and TC-04, however, these adsorbents provide excellent separation performance and their ΔC_V values are also very close (see the data in Table 5); in contrast, CF-91 showed relatively inferior separation performance, with a lower adsorption capacity than those of CF-30 and TC-04. In addition, the separation performance of CF-80 was not desirable, and showed a dynamic separation effect in the forward depressurization stage, with a very low concentration rate of only 7% for CH_4, which further indicates that a larger adsorption selectivity parameter does not imply a better separation performance. The α_{CH_4,N_2} values of the commercial activated carbon samples were between 2-3, and they were able to separate the CH_4/N_2 mixture. The selectivity parameters of CF-30 and TC-04 were higher than those of RX3 and RB3, but the PSA experiment results showed that the concentration rates of CH_4 obtained using RX3 and RB3 under the same conditions were 31.6% and 27.7% respectively, which are close to the concentrations obtained using the prepared activated carbon samples. These results also suggest that apart from the selectivity parameter, the adsorption capacity also influences the prediction of the adsorption selectivity parameter; hence, the PSA method provides a feasible way to judge the adsorbent separation performance.

Table 3. Fitting parameters for CF-30 using the Langmuir equation at different temperatures

CF-30	q_m (mmol/g)			b (MPa^{-1})			r		
	278 K	298 K	318 K	278 K	298 K	318 K	278 K	298 K	318 K
N_2	1.30	1.14	0.96	2.60	2.51	1.22	0.999	0.999	0.999
CH_4	2.07	1.81	1.56	6.45	5.11	2.85	0.998	0.998	0.999
CO_2	3.16	2.75	2.63	13.99	10.29	5.03	0.997	0.997	0.998

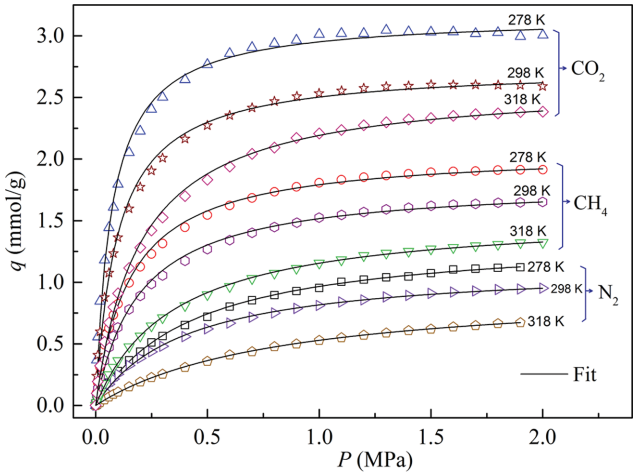

Fig. 3. Adsorption isotherms of CF-30 activated carbon for CH_4, N_2, and CO_2 at 278 K, 298 K, and 318 K.

α_{CO_2,N_2} of the CF-30, TC-04, and CF-91 samples were all >7, while that of CF-80 was only 2.27, showing that only the first four samples are able to separate CO_2/N_2 in an economical way. For the CO_2/CH_4 mixture, α_{CO_2,CH_4} values of CF-30, TC-04 and CF-91 were nearly identical, at around 3, and that of CF-80 was as high as 21.84. Thus, all four samples can technically separate CO_2/CH_4, although the actual separation efficiency of each sample for CO_2/N_2 and CO_2/CH_4 still needs to be verified by conducting PSA experiments.

3. Influence of Adsorption Temperature

Among the prepared samples, CF-30 has the best comprehensive performance, the most stable preparation process and low energy consumption. Using CF-30 as the representative adsorbent, the adsorption isotherms of CH_4, N_2, and CO_2 at 278 K, 298 K, and 318 K were measured, with the results shown in Fig. 3. It is evident that the order of the adsorption capacity was still CO_2>CH_4>N_2, and that at a given pressure, the adsorption capacities of CH_4, N_2, and CO_2 all decreased with increasing temperature.

Langmuir fitting was performed for the adsorption isotherms at the three temperatures, and the obtained parameters are shown in Table 3. As the results show, q_m and b both decreased with increasing temperature, which indicates that the temperature is inversely correlated with the slope of the adsorption isotherms at the initial stage, thereby affecting the adsorption selectivity parameter values. Table 4 provides the selectivity parameter values at different temperatures.

Table 4 shows that α_{CH_4,N_2} at the three temperatures all range between 3 and 4, indicating that the CF-30 sample separates the CH_4/N_2 mixture well in this temperature range. However, α_{CH_4,N_2} has a minimum value at 298 K, and α_{CO_2,N_2} also shows the same trend. On the other hand, α_{CO_2,CH_4} is stable at ~3 in this temperature range. These results indicate that CF-30 can separate the CO_2/CH_4 mixture within this temperature range, and that lower temperatures are more conducive to improving the separation effect.

Table 4. Adsorption selectivity parameters of CF-30 for CH_4, N_2, and CO_2 at different temperatures

T	α_{CH_4,N_2}	α_{CO_2,N_2}	α_{CO_2,CH_4}
278 K	3.95	13.1	3.31
298 K	3.23	9.89	3.06
318 K	3.80	11.29	2.97

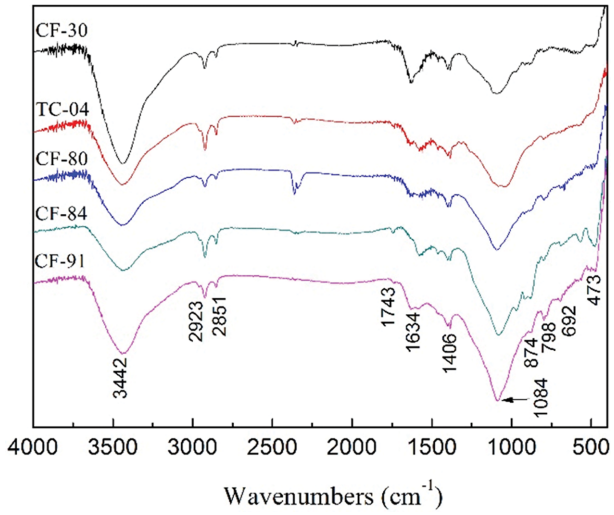

Fig. 4. Infra-red spectra of the CF-30, TC-04, CF-80, CF-84, and CF-91 activated carbon samples.

4. Surface Chemical Properties of Activated Carbon Samples

Fig. 4 shows the infrared spectra of the activated carbon samples. The peak at 3,440 cm^{-1} corresponds to the O-H stretching vibrations, the peak at 2,925 cm^{-1} corresponds to the absorption peak of hydrogen on aliphatic hydrocarbon and naphthene groups, the peak at 2,852 cm^{-1} arises from the addition of KBr to the samples, the peak at 1,380 cm^{-1} corresponds to the bending vibration of methyl, the peak at about 1,600 cm^{-1} corresponds to the stretching vibration of C=C bond in aromatic rings, the absorbance band at 1,070-1,090 cm^{-1} corresponds to C-O stretching vibration, the absorbance band at 1,040-910 cm^{-1} corresponds to minerals or ash, and the absorbance band at 753-743 cm^{-1} corresponds to the planar vibrations of substituted aromatic compounds or methylene.

Fig. 4 shows that, although different preparation techniques were used for the different samples, their infrared spectra are very simi-

lar, indicating that the physical activation method has little effect on the types of functional groups on the surface of the samples. The main structure of GAC is composed of multiple aromatic rings linked with oxygen-containing functional groups including methyl, methylene, carboxyl, and hydroxyl. For all these samples, the absorption peak at 1,100 cm^{-1} noticeably widens, indicating that each sample contains many oxygen-containing functional groups (which are mainly C-O bonds). The reason for the generation of oxygen-containing functional groups can be summarized as follows: first, the pre-oxidation process increases the number of oxygen-containing functional groups on the surface of activated carbon. Second, the carbonization process promotes the condensation polymerization of coal, which increases the content of highly substituted aromatic rings and removes the ash in raw coal. Finally, the

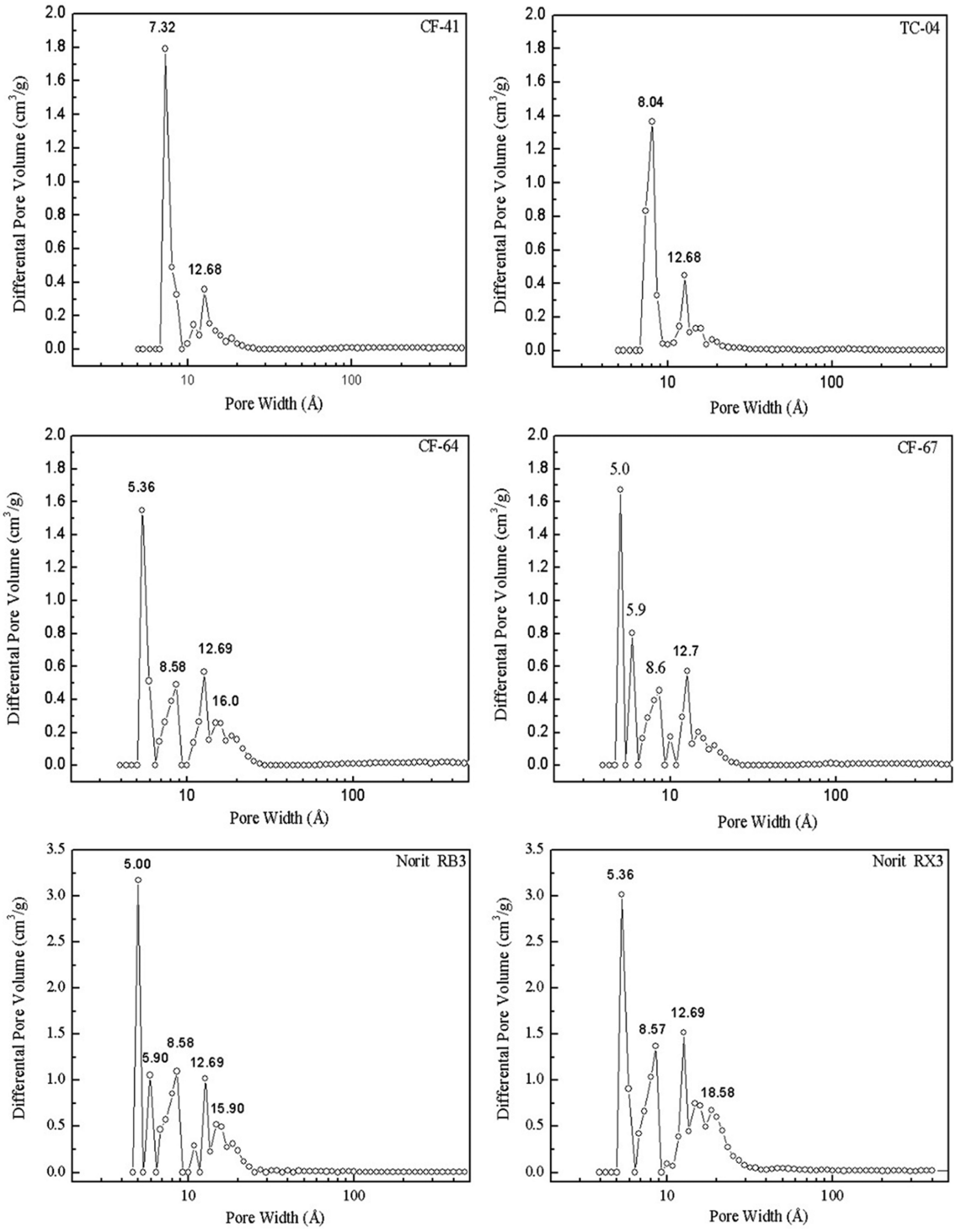

Fig. 5. Pore size distributions of the CF-41, TC-04, CF-64, CF-67, RX3, and RB3 samples activated by water vapor.

Table 5. Pore structure parameters and PSA concentration rate (ΔC_V) of the GAC samples activated by water vapor

Sample	S_{BET} (m^2/g)	S_{mic} (m^2/g)	V_t (cm^3/g)	V_{mic} (cm^3/g)	ΔC_V (vol%)
CF-30	426.49	365.89	0.217	0.169	30.7
TC-04	334.69	273.30	0.170	0.126	31.0
CF-28	391.86	305.15	0.227	0.141	27.4
CF-41	340.01	294.73	0.174	0.136	31.5
CF-64	492.62	378.46	0.258	0.175	32.3
CF-67	479.19	403.49	0.246	0.187	33.5
RX3	1,238.20	809.95	0.653	0.372	31.6
RB3	898.42	728.78	0.440	0.336	27.7

injection of the activated gas can break the chemical bonds that connect the carbon network and cause further changes in the surface functional groups.

5. Pore Structure of GAC

5-1. Effect of Water Vapor Activation on the Pore Structure of GAC

Of the samples prepared by water vapor activation maintained for 1-4 h at 800-950 °C TC-04, CF-41, CF-64, and CF-67 all had ΔC_V values >30% for CH_4 in the CH_4/N_2 mixture, implying very good separation performance. In addition, the pore structures of the commercial activated carbon samples RX3 and RB3 were also characterized and compared with those of the prepared samples. The pore structure parameters and pore size distributions of the samples are given in Table 5 and Fig. 5, respectively. The results show that the pore sizes of both the prepared and the commercial activated carbon samples were mainly distributed in the microporous range, and that the specific surface areas and micropore volumes of the commercial activated carbon were significantly higher than those of the prepared samples.

5-2. Effect of CO_2 Activation on the Pore Structure of GAC

Here, analysis of the samples CF-80, CF-81, CF-82, CF-94, CF-91, and CF-84 is presented. Of these, CF-84 was prepared through the combined activation of water vapor and carbon dioxide, while the others were activated by carbon dioxide alone. The pore structure parameters and ΔC_V values of the samples are shown in Table 6. These results show that the BET specific surface areas of CF-80, CF-81, CF-82, and CF-94 were low, resulting in poor (CF-80 and CF-81) or no (CF-82 and CF-94) separation. The specific surface area of the CF-91 sample activated by CO_2 was significantly lower than that of the sample activated by water vapor, while the pore structure parameters of the CF-84 sample activated through the combination of water vapor and carbon dioxide were very similar to those of the sample activated by water vapor alone. Hence, it may be inferred that the addition of carbon dioxide does not change the pore structure of the samples, and that the activation effect of water vapor is stronger than that of carbon dioxide.

Fig. 6 shows the pore size distributions of the samples activated by CO_2, where it can be seen that the pore size distribution of each sample is consistent with the adsorption rules reflected by its adsorption isotherm. The results show that only medium and large pores were detected in CF-80, and the pore volume contribution of these pores was very small; for CF-81, CF-82, and CF-94, however, micropores <15 Å were detected, and a certain amount of macropores were also detected. In the case of CF-91 and CF-84, the pores were mainly micropores, and the pore size distribution of CF-84 was very similar to that of CF-67.

The prepared activated carbon is rich in microporous structure (<20 Å) because carbonization causes the non-carbon elements to escape in the form of volatiles, thus forming carbon enriched semicoke products. Because the reaction rate of the internal surface area is far less than the diffusion rate of the pore size, so the activation of more moderate water vapor or carbon dioxide, expands the porosity and specific surface area of the activated carbon, but also ensures that the pore size of the activated carbon is more uniform.

5-3. Relationship between Separation Performance and Pore Structure

The separation performance and pore structure data of representative samples are given in Table 7. RX3 and RB3 are commercial activated carbons with high specific surface area, but their separation performance is similar to the prepared samples CF-30, CF-41, TC-04 and CF-84, etc. Table 7 shows that the activated carbons with relatively higher specific surface areas all showed higher separation performance. However, through comparing the micropore surface areas and volumes of micropore all the samples, it can be deduced that, while important, the specific surface area and

Table 6. Pore structure parameters and PSA concentration rates (ΔC_V) for the GAC samples activated by CO_2

Sample	S_{BET} (m^2/g)	S_{mic} (m^2/g)	V_t (cm^3/g)	V_{mic} (cm^3/g)	ΔC_V (vol%)
CF-80	3.99	4.33	0.007	0	7.0
CF-81	97.22	89.42	0.053	0.041	4.0
CF-82	57.83	53.01	0.034	0.024	0.
CF-94	16.22	14.13	0.013	0.006	0.
CF-91	211.62	176.01	0.153	0.081	23.4
CF-84	345.29	299.14	0.177	0.138	30.4

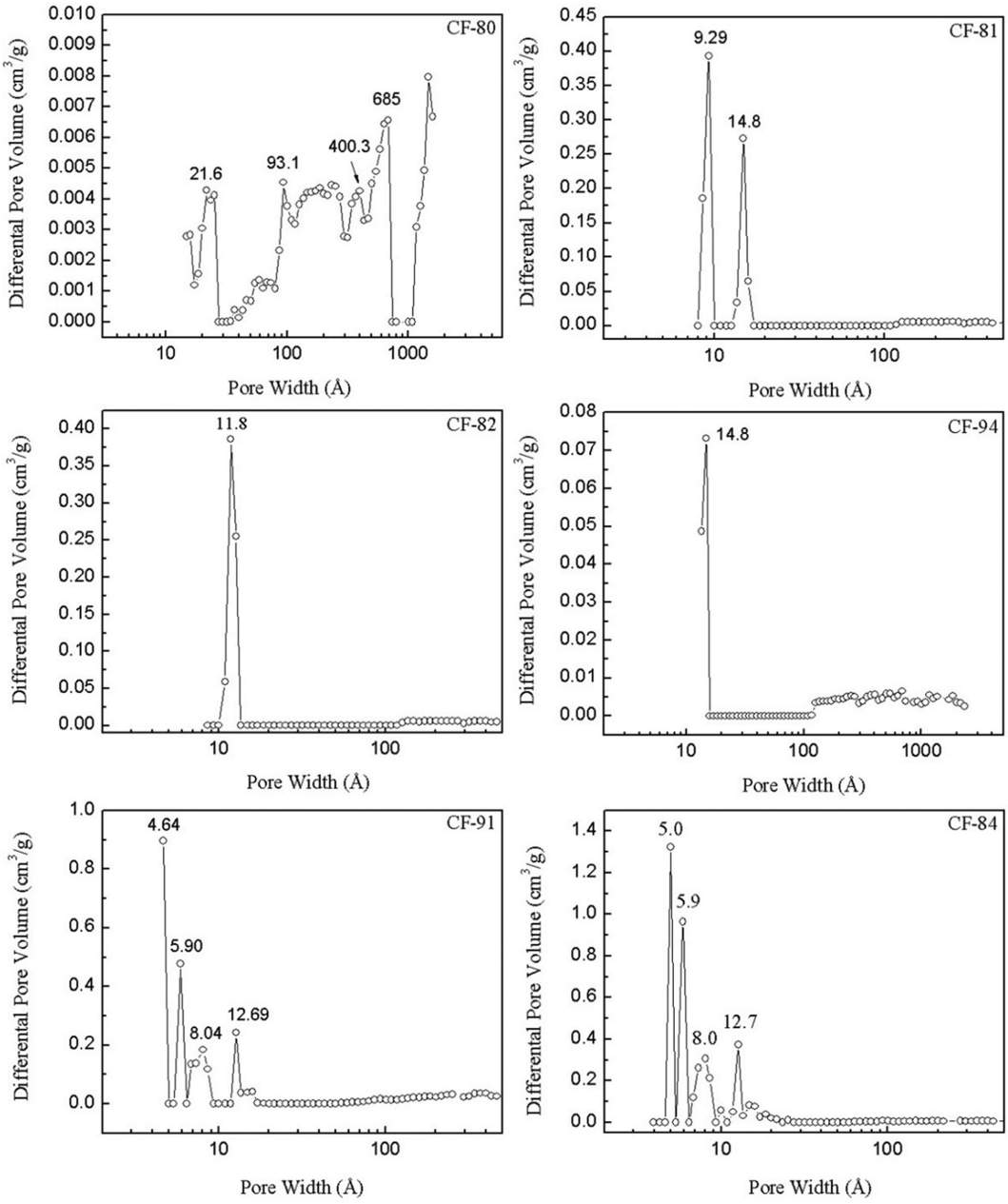

Fig. 6. Pore size distributions of the CF-80, CF-81, CF-82, CF-94, CF-91, and CF-84 samples activated by CO_2.

pore volume of micropores are not the decisive factors in determining the gas separation performance.

For example, the S_{BET} values of CF-80, CF-81, CF-82, and CF-94 were all <100 m^2/g, and these samples showed poor or even no separation effects; on the other hand, the S_{BET} values of CF-64 and CF-67 were in the range of 470-500 m^2/g, and their ΔC_V values reached as high as 33%, and the S_{BET} values of CF-30, TC-04, CF-41, and CF-84 were in the range of 330-430 m^2/g, and their ΔC_V values were all in the range of 30-32%.

Lastly, the S_{BET} value of CF-91 was only 211.62 m^2/g, which was significantly lower than those of the samples with high specific surface area such as CF-30, and its ΔC_V value, at 23.4%, was ~10% lower than the sample with the best separation effect. These results indicate that the specific surface area and pore volume, V_t, both have a significant influence on the separation performance.

Notably, the values of S_{BET} and V_t for RX3 were 3.6 times and 2.7 times those of CF-41, respectively, while their ΔC_V values were the same, while for RB3, the values of S_{BET} and V_t were 2.3 times and 1.0 times those of CF-28, respectively, while their ΔC_V values were similar. This shows that while RB3 has a high specific surface area and a large micropore volume, its ΔC_V value is only 27.7%.

The kinetic diameters of CH_4 and N_2 are 0.380 nm and 0.364 nm, respectively [33]. In the process of separating gas mixtures, if the pores of the adsorbent are just large enough to allow the CH_4 molecules to enter but too small to allow N_2 molecules to enter, the mixture can be separated. Thus, the adsorption selectivity is depen-

Table 7. Pore size, pore size distribution range, cumulative pore volume, and PSA concentration rate (ΔC_V) of activated carbon samples

Sample	Pore size peak (Å)	Pore range corresponding to pore size peak (Å)	Cumulative pore volume $V\times10^3$ (cm^3/g)	Cumulative surface area S (m^2/g)	ΔC_V (vol%)
CF-28	5.89	5.36-6.43	92.32	311.14	27.4
	8.57	6.79-9.29	20.78	52.00	
	12.68	9.29-17.16	23.38	34.58	
CF-30	5.89	5.36-6.43	88.66	300.68	30.7
	8.57	6.79-9.29	27.61	68.34	
	12.68	9.29-17.16	34.38	53.73	
TC-04	8.04	6.79-10.00	90.27	229.30	31.0
	12.68	10.00-17.16	33.88	51.12	
CF-41	7.32	6.79-9.29	92.82	245.21	31.5
	12.68	9.29-17.16	33.25	51.69	
CF-64	5.36	5.00-6.43	75.55	274.95	32.3
	8.58	6.43-9.29	42.56	107.69	
	12.68	10.00-13.58	36.38	59.12	
	15.91	13.58-29.49	39.57	45.20	
CF-67	5.00	4.65-5.36	51.94	207.61	33.5
	5.89	5.36-6.43	31.87	108.07	
	8.58	6.43-9.29	38.33	109.19	
	12.68	10.00-27.34	62.21	91.40	
RX3	5.36	5.00-6.43	143.8	523.98	31.6
	8.57	6.43-9.29	111.3	290.55	
	12.69	9.29-14.83	106.0	163.27	
	18.58	14.83-40.03	125.3	127.32	
RB3	5.00	4.65-5.36	98.61	394.11	27.7
	5.89	5.36-6.43	41.83	141.91	
	8.58	6.43-9.29	98.01	249.62	
	12.69	9.29-13.58	49.30	79.61	
	15.9	13.58-40.03	70.13	81.01	
CF-80	21.62	17.16-27.34	0.57	0.78	7.0
	93.11	79.88-117.23	0.57	0.12	
	185.86	117.23-294.51	1.63	0.16	
	684.99	317.92-739.68	1.30	0.07	
CF-81	9.29	8.04-10.00	19.00	41.95	4.0
	14.83	12.68-17.16	12.56	16.89	
CF-82	11.79	10.00-13.58	22.65	37.76	0
CF-94	14.83	3.93-4.29	4.37	6.13	0
CF-91	4.64	4.64-5.00	28.90	124.38	23.4
	5.90	5.36-6.43	18.93	64.19	
	8.04	6.43-9.29	18.95	49.56	
	12.68	11.79-17.16	11.40	17.09	
CF-84	5.00	4.65-5.36	41.15	164.48	30.4
	5.90	5.36-6.43	38.19	129.52	
	8.04	6.43-9.29	30.06	77.60	
	12.69	10.00-25.20	25.19	37.21	

dent on the pore size. Pore structure plays a role in screening gas molecules. As Fig. 6 and Table 7 show, the pore size distribution diagram of CF-94 has a peak at 14.8 Å, while its ΔC_V value is 0, indicating that the pores larger than this size cannot separate the CH_4/N_2 mixture; on the other hand, CF-82 contains a certain number of pores around 11.8 Å, but has too low a specific surface area

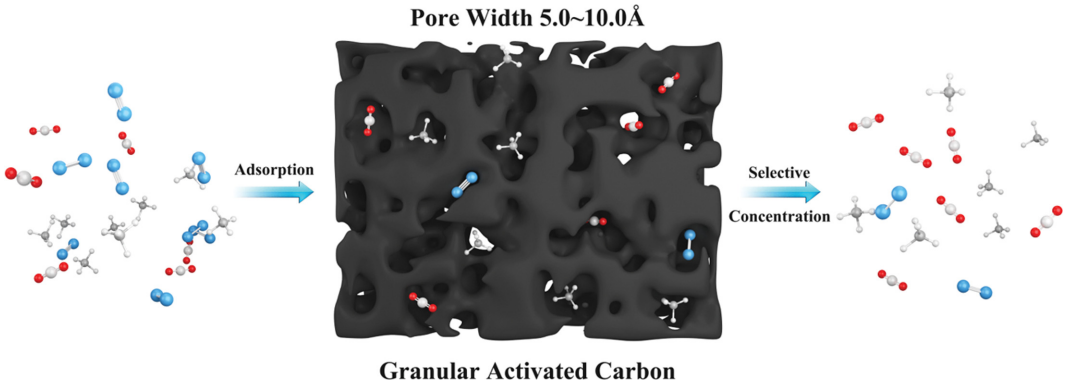

Fig. 7. Influence of pore structure of GAC on the adsorption of CO_2, CH_4 and N_2.

and too small a pore volume to separate CH_4/N_2, resulting in a ΔC_V value of 0; further, CF-81 mainly has 9.29 Å pores and shows some separation effect, while CF-80 has a special pore size distribution and a slightly larger ΔC_V value than CF-81, and its microporous structure plays some role in the separation of the CH_4/N_2 gas mixture. Through analyzing the pore size distributions of the samples, it is evident that the samples with pores <9.0 Å showed better separation performance. This result is consistent with Kuson [34], who found that for pores <13 Å the selectivity parameters for CH_4/N_2 were always >3.0.

CF-41 and TC-04 both have pores in the range of 6.7-10.0 Å, with pore volumes very close to each other, and ΔC_V values >30%. CF-30, CF-64, CF-67, CF-28, and CF-84 share some commonalities, in that while the number (or volume) of pores in the 6.7-10.0 Å range was less than for CF-41 and TC-04, they contain a larger proportion of pores in the range of 5.0-6.7 Å, and their ΔC_V values are >27%. RX3 and RB3 also showed similar results. Zhao et al. [35] found that 0.758-0.776 nm pores showed the best separation effect for the CH_4/N_2 gas mixture, and Kluson et al. [34] believed that the best separation effect was obtained with0.7-0.9 nm pores.

The results obtained in the present study, however, indicate that pores in the size range of 5.0-10.0 Å show the best separation effect for the CH_4/N_2 mixture, and that the pore size distribution of activated carbon is the decisive factor affecting its separation performance.

CONCLUSIONS

A series of granular activated carbon (GAC) samples were prepared from anthracite via both water vapor and carbon dioxide activation. First, the samples were used as adsorbents to test the PSA separation performance for the CH_4/N_2 gas mixture, and the concentration rates, ΔC_V, of CH_4 were obtained. Next, the adsorption isotherms of N_2, CH_4, and CO_2 were determined, and the adsorption selectivity parameters were obtained. Finally, the pore structure and surface functional groups of the prepared activated carbon were characterized. From these results, it may be concluded that the pore size distribution of GAC is the primary factor affecting the concentration effect on CH_4 or CO_2.

Using the GAC sample with the best performance as the adsorbent, the concentration of CH_4 in the CH_4/N_2 gas mixture could be increased to 63.5% by utilizing the single-column single-cycle PSA process. However, there is still room for improvement in the specific surface areas and porosities of the prepared samples relative to those of commercial activated carbon samples. The selectivity parameters for CH_4/N_2 and CO_2/CH_4, i.e., α_{CH_4,N_2} and α_{CO_2,CH_4}, of the sample with the best PSA separation effect, were 3.23 and 3.06, respectively, and the separation process was economical; however, a higher selectivity parameter did not always result in a better separation performance. It was found that low temperatures were more conducive to improving the separation effect, and that the pore size distribution of granular activated carbon samples with the best performance was dominated by micropores, with specific surface areas in the range of 330-500 m^2/g, and micropore volumes in the range 0.12-0.19 cm^3/g. In addition, the surface chemical properties, specific surface area, and pore volume of micropores of the GAC samples also played a role in the determining the separation performance. Overall, however, it was the pore size distribution rather than the specific surface area or pore volume which was the decisive factor in the separation performance. The concentration rate of CH_4 or CO_2 in the gas mixture could be effectively improved by increasing the proportion of micropores with sizes in the range of 5.0-10.0 Å. As Fig. 7 shows, micropores of 5.0-10.0 Å have a significant sieving effect, which can significantly increase the concentration of CH_4 and CO_2 molecules in the adsorption and separation process. In future research, both the process for increasing the proportion of micropores in GACs and the resulting effects on the absorption mechanism will be further investigated.

The results from this study will make it possible to upgrade the preparation process of GACs, thereby lowering costs and improving the efficiency of processes such as methane purification, flue gas treatment, and air pollution control.

ACKNOWLEDGEMENTS

This work was supported by Chongqing Basic Science and Advanced Technology Research Program (Grant No. cstc2017jcyjAX0266), Chongqing Science and Technology Commission Projects (Grant No. cstc2018jcyj-yszxX0005, and cstc2020yszx-jcyjX0008), Natural Science Foundation Project of Chongqing (Grant No. cstc2020jcyj-msxm1228).

REFERENCES

1. Y. Fan, C. Deng, X. Zhang, F. Li, X. Wang and L. Qiao, *Int. J. Greenh. Gas Control.*, **12**, 76 (2018).
2. S. J. Doong and R. T. Yang, *AICHE J.*, **397**, 32 (1986).
3. V. G. Gomes and K. W. K. Yee, *Sep. Purif. Technol.*, **161**, 28 (2002).
4. D. Lozano-Castelló, M. A. Lillo-Ródenas, D. Cazorla-Amorós and A. Linares-Solano, *Carbon*, **741**, 39 (2001).
5. A. R. Yacob and H. M. A. Swaidan, *Appl. Mech. Mater.*, **2124**, 110 (2012).
6. B. Buczek, *Chem. Process Eng-Inz.*, **385**, 21 (2000).
7. P. Brea, J. A. Delgado, V. I. Águeda and M. A. Uguina, *Sep. Purif. Technol.*, **61**, 179 (2017).
8 G. Sethia and A. Sayari, *Carbon*, **68**, 93 (2015).
9. A. Rehman, Y. Heo, G. Nazir and S. Park, *Carbon*, **71**, 172 (2021).
10. M. Lee, M. Park, H. Kim and S. Park, *Sci. Rep.*, **1**, 6 (2016).
11. L. Wang, L. Rao, B. Xia, L. Wang, L. Yue and Y. Liang, *Carbon*, **31**, 130 (2018).
12. J. Park, N. F. Attia and M. Jung, *Energy*, **9**, 158 (2018).
13. Y. Boyjoo, Y. Cheng, H. Zhong, Y. Hao, J. Pan and V. K. Pareek, *Carbon*, **490**, 116 (2017).
14. R. Ullah, M. A. H. S. Saad, S. Aparicio, S. Aparicio and M. Atilhan, *Micropor. Mesopor. Mater.*, **49**, 262 (2018).
15. M. J. Vaezi, A. A. Babaluo and H. Maghsoudi, *Chem. Eng. Res. Des.*, **347**, 134 (2018).
16. T. T. Trinh, T. S. van Erp, D. Bedeaux, S. Kjelstrup and C. A. Grande, *Chem. Chem. Phys.*, **8223**, 17 (2015).
17. A. Arami-Niya, T. E. Rufford and Z. Zhu, *Carbon*, **115**, 103 (2016).
18. J. M. Rosas, R. Ruiz-Rosas, J. Rodríguez-Mirasol and T. Cordero, *Chem. Eng. J.*, **707**, 307 (2017).
19. M. Gu, B. Zhang, Z. Qi, Z. Liu, S. Duan and X. Du, *Sep. Purif. Technol.*, **213**, 146 (2015).
20. S. Cavenati, C. A. Grande and A. E. Rodrigues, *Sep. Sci. Technol.*, **2721**, 40 (2005).
21. F. Notaro, J. T. Mulhaupt, F. W. Leavitt and M. W. Ackley, US Patent, 5,810,909 (1998).
22. S. U. Rege and R. T. Yang, *Sep. Sci. Technol.*, **3355**, 36 (2001).
23. S. U. Rege and R. T. Yang, *Chem. Eng. Sci.*, **3781**, 56 (2001).
24. H. W. Habgood, *Can. J. Chem.*, **1384**, 36 (1958).
25. D. M. Ruthven, S. Farooq and K. S. Knaebel, Pressure Swing Adsorption, Wiley-VCH (1994).
26. M. Gu, University of Chong Qing China, PhD thesis (2000).
27. M. S. A. Baksh, R. T. Yang and D. D. L. Chung, *Carbon*, **931**, 27 (1989).
28. L. Zhou, W. C. Guo and T. P. Zhou, *Chin. J. Chem. Eng.*, **558**, 10 (2002).
29. H. Ruan, University of Tian Jin China, PhD thesis (2010).
30. F. Foeth, M. Andersson, H. Bosch, G. Aly and T. Reith, *Sep. Sci. Technol.*, **93**, 29 (1994).
31. R. V. Jasra, N. V. Choudry and S. G. T. Bhat, *Sci. Technol.*, **885**, 26 (1991).
32. D. M. Ruthven, *Principles of adsorption and adsorption processes*, John Wiley & Sons Publications, New York (1984).
33. X. J. Cui, R. Marc Bustin and G. Dipple, *Fuel*, **293**, 83 (2004).
34. P. Kluson, S. Scaife and N. Quirke, *Sep. Sci. Technol.*, **15**, 20 (2000).
35. G. F. Zhao, P. Bai, H. M. Zhu, R. X. Yan, X. M. Liu and Z. F. Yan, *Asia-Pac. J. Chem. Eng.*, **284**, 3 (2008).